Impact of Agricultural Practice on Regional Climate in a Coupled Land Surface Mesoscale Model

H.S. Cooley

Energy and Resources Group, University of California at Berkeley,

Berkeley, CA

Earth Sciences Division, Lawrence Berkeley National Laboratory,

Berkeley, CA

W.J. Riley and M.S. Torn

Earth Sciences Division, Lawrence Berkeley National Laboratory,

Berkeley, CA

Y. He

Computational Research Division, Lawrence Berkeley National Laboratory,

Berkeley, CA

1. Abstract

The land surface has been shown to form strong feedbacks with climate due to linkages between atmospheric conditions and terrestrial ecosystem exchanges of energy, momentum, water, and trace gases. Although often ignored in modeling studies, land management itself may form significant feedbacks. Because crops are harvested earlier under drier conditions, regional air temperature, precipitation, and soil moisture, for example, affect harvest timing, particularly of rain-fed crops. This removal of vegetation alters the land surface characteristics and may, in turn, affect regional climate. We applied a coupled climate (MM5) and land-surface (LSM1) model to examine the effects of early and late winter wheat harvest on regional climate in the Department of Energy Atmospheric Radiation Measurement (ARM) Climate Research Facility in the Southern Great Plains, where winter wheat accounts for 20% of the land area. Within the harvested, winter wheat region, simulated 2 m air temperature was 1.3^{o}C warmer in the Early Harvest scenario at mid-day averaged over the two weeks following harvest. Soils in the harvested area were drier and warmer in the top 10 cm and wetter in the 10–20 cm layer compared to those in the Late Harvest. Midday soils were 2.5^{o}C warmer in the harvested area at mid-day averaged over the two weeks following harvest. Harvest also dramatically altered latent and sensible heat fluxes. Although differences between scenarios diminished once both scenarios were harvested, the short-term impacts of land management on climate were comparable to those from land cover change demonstrated in other studies.

2. Introduction

One of the most significant ways in which humans have modified ecological systems is via land use and land cover change [*Vitousek*, 1994]. Impacts occur from local to global scales and include loss of biodiversity, disruption of biogeochemical cycles, erosion, disruption of the fire regime, and climate change [*Vitousek*, 1994; Ostlie, 1997].

The Great Plains of the United States have experienced extensive land cover modification. Due to rich soil and favorable climate, vast tracts have been converted from prairie to managed agriculture. Historically, the prairie in this region extended over 2.6 million km^2, from Canada to Mexico and the foothills of the Rockies to Indiana [*Ostlie*, 1997]. The extent of land-surface modification increases from west to east. Between 82 and 99% of the tallgrass prairie, predominately found in the eastern section of the Great Plains, has been converted [*Samson and Knopf*, 1994]. Using Advanced Very High Resolution Radiospectometry (AVHRR) 1-km satellite data, Loveland and Hutcheson [1995] estimate that 25% and 90% of historical short- and tallgrass prairie, respectively, were under cultivation by 1990.

Vegetation influences climate through land surface properties, e.g., albedo, surface roughness, rooting depth, leaf area index, and canopy resistance [*Pielke and Avissar*, 1990] over a range of spatial and temporal scales [*Pielke*, 1993; *Pielke et al.*, 1998]. These land-surface characteristics vary by land-cover type. Thus anthropogenic modification of vegetation alters these characteristics and consequently climate. The specific effect of conversion to cropland depends on the crop type and its properties in comparison with those of the land cover type that it replaces. In addition, human modification affects landscape heterogeneity, which observational and modeling studies

have shown may induce or modify mesoscale circulations [*Segal et al.*, 1998].

Throughout sections of the Great Plains, the dominant agricultural crop is winter wheat, which is planted in early fall and harvested in June or July. This pattern contrasts sharply with the seasonal cycle of prairie grasses, which are most active from June to September. We expect that the change from prairie to winter wheat alters the magnitude and seasonal timing of energy, momentum, water, and carbon fluxes between the atmosphere and ecosystem. McPherson et al. [2004] showed a striking discontinuity in visual greenness between the winter wheat region in Oklahoma and the surrounding vegetation and argued that these changes impact maximum daily near-surface air temperature and dewpoint. Using data from automated Mesonet sites throughout Oklahoma, they detected a summer warming and winter cooling in the winter wheat region relative to the surrounding area. In a study combining modeled and observational data of July conditions in Oklahoma, Weaver and Avissar [2001] demonstrated that landscape heterogeneity, such as that associated with intermixed winter wheat and other crops, was sufficient to induce vertical velocities of 1–2 m s^{-1}. Their simulated vertical velocity patterns coincided with satellite observations of cloud formation, implying that these enhanced vertical velocities were sufficient to induce convective cloud formation.

Modeling sensitivity experiments provide a means to evaluate the effect of land-surface characteristics on regional and global climate. In traditional force-response sensitivity experiments, the value of one variable of the model environment is altered and results are compared to a control scenario, providing an indication of the forcing potential of a single land-surface characteristic on climate. As reviewed by Pielke et al. [1998] and Garratt [1993], these sensitivity studies indicate that land-surface characteristics can

affect regional and global climate. The single factor analysis, however, cannot resolve the more realistic case of multiple factors changing simultaneously, which often occurs with land cover modification.

Climate and land-cover modifications result in simultaneous changes in many system state variables, and thus evaluating the net positive or negative feedback requires an integrated analysis. Over the past ten years, coupled atmosphere and land surface models have been developed, allowing a quantitative exploration of these interactions. The effect of land cover change on the climate of the United States has been studied by comparing current, historical, and in some cases, future land cover scenarios [*Bonan*, 1997; *Bonan*, 1999; *Bounoua et al.*, 2002; *Copeland et al.*, 1996; *DeFries et al.*, 2002; *Pan et al.*, 1999]. These studies reported regional and seasonal differences in response to land cover change. Bounoua et al. [2002] demonstrated that conversion from forest to cropland produced a cooling in temperate latitudes and a warming in the tropics. DeFries et al. [2002] projected that future land cover conversion will be concentrated in the tropics and subtropics, and conversion will warm these regions. Studies centered on the United States have found that historical land cover change, particularly the conversion of forest to cropland, has produced a cooling in the central and eastern United States and a warming in the western United States [*Bonan*, 1997; *Bonan*, 1999; *Pan et al.*, 1999]. Bonan [1997; 1999] showed that modeled response was greatest during the summer months and diminished in fall when crops have been harvested and trees have lost their leaves. Pan et al. [1999] further demonstrated that the land surface-climate system response was not sensitive to climate regime (i.e., normal, flood, or drought conditions) for any climate parameters considered (i.e., latent and sensible heat fluxes and surface air

temperature) except precipitation.

Within a particular land cover type, land management may also affect land surface-climate interactions. Regional modeling studies are required to address land management because the spatial heterogeneity of agricultural practices cannot be captured at the scale of GCM grid cells. In a regional modeling study, Segal et al. [1998] found that irrigation resulted in an increase in precipitation in non-irrigated areas, but did not produce any new rainfall areas. Similarly, Chase et al. [1999], in a study corroborated by historical data, found that irrigation in the northern Colorado plains impacted climate in the plains and in the adjacent mountains. Other management factors, such as nitrogen addition and harvest timing, may also be important but have not yet been explicitly addressed. Harvest should influence climate because removal of vegetation decreases albedo, surface roughness, leaf area index, and canopy resistance.

The potential for feedback between atmospheric conditions and land management exists because some of the climate-forcing practices are themselves responses to climate. Air temperature, precipitation, and soil moisture, for example, affect harvest timing, particularly for rain-fed crops. Crop growth and grain development depend on season-long environmental conditions, such as cumulative degree days, cumulative and episodic precipitation, and cumulative photosynthetically active radiation. During dry conditions, crops mature earlier, thereby forcing an earlier harvest. Because combines are expensive to purchase, winter wheat is harvested by combine crews that begin in Texas and migrate northward to Canada. As a result, harvest tends to be temporally coherent with potential regional climate implications.

In this paper we examine the extent to which an early harvest affects regional

climate by applying a coupled climate (MM5) and land surface model (LSM1). We apply the coupled model in the Department of Energy's Atmosphere and Radiation Measurement (ARM) Climate Research Facility (ACRF; previously named the Cloud and Radiation Testbed - CART) in the Southern Great Plains (hereafter ARM-SGP). We focus here on winter wheat because it is an important agricultural crop in the Central and Southern Great Plains and is found in a nearly contiguous belt from southern Nebraska to northern Texas. Two two-month long simulations are performed: the first with an early winter wheat harvest in June, and the second with a late harvest in July. Spatial and temporal patterns of land-surface conditions and exchanges and near-surface atmospheric conditions are compared between the two scenarios.

3. Methods

3.1. *Coupling LSM1 to MM5 and Model Testing*

We have integrated the land-surface model LSM1 [*Bonan*, 1996] into the meteorological model MM5 [*Grell et al.*, 1995] to simulate the coupled interactions of water, energy, and CO_2 exchanges between plants and the atmosphere. LSM1 has several advantages over the most sophisticated land-surface model (OSULSM [*Chen and Dudhia*, 2001a; *Chen and Dudhia*, 2001b]) currently implemented in the publicly available version of MM5. The OSULSM uses a Penman potential evaporation approach, a relatively simple canopy resistance model, and has no ability to simulate changing plant leaf area.

In contrast, LSM1 is a "big-leaf" [*Dickinson et al.*, 1986; *Sellers et al.*, 1996], single-canopy land surface model that simulates CO_2, H_2O, and energy fluxes between ecosystems and the atmosphere. Modules are included that simulate aboveground fluxes

of radiation, momentum, sensible heat, and latent heat; energy and water fluxes below ground, and coupled CO_2 and H_2O exchange between plants and the atmosphere. Twenty-eight surface types, comprising varying fractional land covers of thirteen plant types, are simulated in the model. Soil hydraulic characteristics are determined from sand, silt, and clay content. LSM1 has been tested in a range of ecosystems at the site level (e.g., [*Bonan et al.*, 1995; *Bonan et al.*, 1997; *Riley et al.*, 2003]) and accurately predicts carbon, latent heat, and sensible heat fluxes under a variety of conditions.

LSM1 requires as input above-canopy air temperature, wind speed, CO_2 concentration, vapor pressure, downward diffuse and direct shortwave radiation, downward longwave radiation, and precipitation or irrigation amount. These variables are available in the interface between the atmosphere and current land-surface submodels in MM5, with the exception of the partitioning of incoming solar radiation between direct and diffuse and visible and near-infrared components. We applied the CCM2 version of the atmospheric radiation code currently in MM5 to produce these radiation inputs. In the interface between the land surface and atmospheric models we converted vegetation and soil types from the USGS vegetation classes as used in MM5 to those used in LSM1.

We tested the coupled MM5-LSM1 model by comparing simulation results to data collected during the First International Satellite Land Surface Climatology Project Field Experiment (FIFE) campaign [*Betts and Ball*, 1998] and to simulations using the OSULSM. These comparisons are similar to those made by Chen and Dudhia [2001b] for the OSULSM. The FIFE experiments were conducted over a 15×15 km area of the Konza prairie in Kansas during 1987–1989. In the comparisons we applied the 30-minute spatial averages over the study area for three months each in 1987, 1988, and 1989. We present

results for sensible, latent, and ground heat fluxes and 2 m air and surface skin temperature predictions.

3.2. *MM5/LSM1 Simulations*

We used the standard initialization procedure for MM5, which applies first-guess and boundary condition fields interpolated from NCEP reanalysis data to the outer computational grid. Simulations were performed with a coarse grid of 100×100 km horizontal resolution (54×68 grid points) spanning the 48 contiguous states and one-way nesting to 10×10 km horizontal resolution (41×41 grid points) for the approximate 3°×3° area of the ARM–SGP region. The fine grid was centered over the FIFE area for testing and centered over the ARM-SGP region for the June and July harvest simulations. In the vertical direction we used 18 σ-layers between the 100 mb level and earth's surface. The following physics packages were used in the simulations: Grell convective scheme, simple ice microphysics, MRF PBL scheme, and the CCM2 radiation package.

Because this study used one-way nesting between the 100 and 10 km horizontal resolutions, changes resulting from harvest in the ARM-SGP 10 km grid area were not communicated back to the surrounding continental area. Although Lu et al. [2001] discussed the importance of two-way nesting in climate models, we feel that one-way nesting was appropriate in our study. Because changes associated with harvest are concentrated within the harvested region with little effect on the surrounding area, it is unlikely that harvest would have significantly altered climate outside of the ARM-SGP. Thus, one-way nesting would have little effect on all climate variables considered in this study, with the exception of precipitation, which we discuss in more detail in section 4.2.

3.3. *Harvest Simulation*

For the harvest simulations, the 10×10 km resolution model grid was centered over the ARM-SGP. Two scenarios were run over the study period, which extended from June 1 to July 31, 1987. In the first scenario, referred to as Early Harvest, all winter wheat in the domain was harvested on June 4, 1987 (Julian Day 155). In the second scenario, referred to as Late Harvest, all winter wheat in the domain was harvested on July 5, 1987 (Julian Day 185). These dates represent the extremes of winter wheat harvest in Oklahoma [*USDA*, 1997b]. Winter wheat is widespread in the region, accounting for 20% of the land area in the ARM-SGP region. Post-harvest residue is burned, left on the soil, or plowed into the soil. For annual crops, such as wheat, residue is typically plowed into the soil (Caddel, personal communication). Thus we simulated harvest by setting the land cover type to bare soil in winter wheat grid cells. We did not consider the impact of remnant stems on albedo or water retention capacity of the soil.

Land cover at the 10×10 km resolution model grid was assigned based on the USGS 1-km AVHRR data obtained from satellite images taken between April 1992 and March 1993. We divided the area that the USGS designated as agricultural land into two categories: winter wheat and other crops, based on data from the 1997 Census of Agriculture [*USDA*, 1997a]. In some counties, the USGS data did not record the presence of crops even though the census data indicated that these counties had substantial crop coverage. The scaling of surface characterization data from the 1 to 10 km scale caused this discrepancy by assigning the most prevalent land surface type among the one hundred 1×1 km grid cells to the 10×10 km grid cell. Thus, specificity of land cover characterization was lost when scaling up to the 10 km scale. To address this problem, we

forced the percent crop and winter wheat in each county to match values calculated from the 1997 census data, thereby creating a new land cover map (Figure 1).

LAI values prescribed by LSM1 look-up tables were used for all land cover types except winter wheat. For winter wheat, we averaged LAI measurements taken between 1997 and 2001 at the AmeriFlux winter wheat site in Ponca City, Oklahoma (Verma, personal communication) (Figure 2). All other secondary vegetation and soil parameter values were prescribed by LSM1 for all land cover types.

4. Results

4.1. *Coupled Model Testing*

To evaluate the coupling between MM5 and LSM1 we performed comparisons with data from FIFE and to simulations using the OSULSM for three months each in 1987, 1988, and 1989. For example, comparisons between measurements and predictions from MM5 coupled with the LSM1 and OSULSM land-surface models during June, 1987 are shown in Figure 3 for: (a) latent heat flux; (b) sensible heat flux; and (c) ground heat flux. The predictions are sensitive to the initial soil moisture, so that comparisons between modeled and measured values were made after a model spin-up of several days. Generally, the LSM1 predictions of surface energy fluxes are as or more accurate than those of the OSULSM land-surface model.

For both models surface skin temperature and 2 m air temperatures were under predicted, by up to 4°C, in the first two weeks after model spin-up (Figure 4). In the final two weeks of June both land-surface models relatively accurately predicted peak surface skin and 2 m air temperatures. Comparisons of this kind between land-surface models

coupled to regional-scale meteorological models can be problematic. For example, errors in simulation of atmospheric processes (e.g., vapor transport, cloud parameterization, radiation dynamics, or PBL dynamics) will propagate to the land-surface model and may distinctly impact the energy exchange predictions of each land-surface model. A second limitation to this test is that the FIFE dataset is calculated as a spatial average over 225 km^2 assembled from data from a limited number of stations (22 in 1987, 10 in 1988, and 14 in 1989). Thus the dataset may not accurately capture the spatial heterogeneity in fluxes present in the area at all times. Still, the FIFE study provides a high-quality dataset to evaluate distributed land-surface models. Comparisons such as those performed here over several seasons and years with varying climate give some confidence that the coupled model can accurately simulate the energy partitioning mechanisms important for land-use change analyses.

4.2. *Harvest Simulations*

We report results as the difference between the Early and Late Harvest scenarios. Therefore comparisons during June represent the difference between a harvested and a non-harvested scenario, and comparisons during July represent the difference between a June harvest and a recently harvested scenario. If, for example, on June 10 at noon, air temperature was warmer in the Early Harvest scenario then in the Late Harvest scenario, the difference between the simulations was positive. Percent change was calculated relative to the Late Harvest scenario. Differences were deemed significant if they exceeded 0.001 $m^3\ m^{-3}$ for soil moisture, 0.1°C for soil and air temperatures, and 3 W m^{-2} for latent and sensible heat fluxes.

Figures 5–8 depict Late Harvest and differences between Early and Late Harvest

for the following variables: latent and sensible heat fluxes, 2 m air temperature, soil temperature, soil moisture in 0–10 cm and 10–20 cm depth layers, and cumulative precipitation. Differences between scenarios were spatially heterogeneous and were largest in the center of the ARM-SGP, where winter wheat is planted in a nearly contiguous belt. Because results varied according to land cover type, we divided the results into two categories: winter wheat and non-winter wheat. Differences between scenarios were thus averaged over the winter wheat and the non-winter wheat land cover types.

Four distinct phases in the system's response were identified based on abrupt changes in energy partitioning. Phases 1, 2, 3, and 4 extended from Julian Days 155–158 (0–3 days after the June harvest), 158–170 (3–15 days after the June harvest), 170–185 (15–30 days after the June harvest), and 185–210 (days 30–55 after the June harvest, or days 0–25 after the July harvest), respectively. We discuss each phase in detail below.

In both scenarios, latent heat flux accounted for the largest portion of net radiation flux from the surface to the atmosphere during Phase 1 (Figure 5). In comparing the effect of early harvest relative to late harvest, midday latent heat flux increased by 99 W m^{-2} (22%), and sensible heat flux decreased by 44 W m^{-2} (-28%) across the winter wheat region. There was no significant difference in midday sensible and latent heat fluxes in the non-winter wheat region. The increase in latent heat flux in the winter wheat region was largest the first day after harvest and declined over the following three days, reflecting a concurrent decline in soil moisture.

Large latent heat fluxes in both scenarios, combined with a lack of precipitation during Phase 1 (Figure 6), resulted in a decline in volumetric soil moisture content, θ (m^3

water m^{-3} soil), in the 0–10 ($\theta_{0–10}$) and 10–20 ($\theta_{0–20}$) cm soil layers in both harvest scenarios (Figure 7). In the winter wheat region, $\theta_{0–10}$ declined by 0.029 m^3 m^{-3} (-11%). There was no significant change in soil moisture in the $\theta_{10–20}$ in the winter wheat region or at any depth in the non-winter wheat region.

In the Early Harvest scenario, vegetation removal eliminated soil surface shading, removed roots that access deeper water, and eliminated transpiration. As a result, all latent heat flux in the harvested region was due to soil evaporation. Because latent heat flux increased during Phase 1, soil evaporation increases were greater than decreases in transpiration. Thus, by shading the soil, vegetation hindered total evapotranspiration during the first few days after harvest. We calculated the reduction in soil water in each soil layer as a percentage of the integrated latent heat flux over the first three days in the winter wheat region. Soil water losses in the 0–10 cm layer as a percentage of integrated latent heat flux were substantially larger in the Early Harvest scenario than in the Late Harvest scenario (55% versus 33%). Thus, harvest shifted the source of evaporated water to the surface soil, resulting in a relatively drier surface layer and a wetter deep layer.

The diurnal 2 m air temperature range declined in the winter wheat region, as the midday temperature decreased by 0.9°C and nighttime temperature increased by 0.3°C. By contrast, the diurnal temperature range of the soil in the winter wheat region increased slightly, with greater cooling at night (1.1°C) than during midday (0.3°C) (Figure 8). There was no significant change in the non-winter wheat region. Although albedo declined as a result of harvest, the change in latent heat flux was substantial enough to cause a net cooling in midday soil and 2 m air temperatures. The nighttime response of the soil and air temperatures was likely a result of vegetation removal, which allowed

heat to escape from the soil at night, effectively warming the air and cooling the soil.

In Phase 2, large differences in all ecosystem stocks and fluxes were evident between the two scenarios. In the winter wheat region, midday latent heat flux declined by 173 W m^{-2} (-45%), and sensible heat flux increased by 124 W m^{-2} (121%) relative to the Late Harvest scenario. The decline in latent heat flux was due to a lack of soil moisture. In the non-winter wheat region, midday latent heat flux increased by 9 W m^{-2} (3%), with no significant change in sensible heat flux relative to the Late Harvest scenario.

A small amount of precipitation occurred in both scenarios at the end of Phase 2, with slightly more (0.04 cm) falling in the Early Harvest scenario. In the Early Harvest scenario, some areas received up to 6 cm more, while others received up to 5 cm less precipitation than in the Late Harvest scenario. The increase in precipitation in the Early Harvest scenario was likely due to the excess latent heat flux and subsequent transport of moisture to the atmosphere from the soils in the harvested region during Phase 1. This precipitation was then redistributed across the ARM-SGP.

Because precipitation was light during Phase 2, soil moisture continued to decline in both simulations, and the difference in $\theta_{0–10}$ and $\theta_{10–20}$ reached a maximum during this period. Large reductions occurred in the winter wheat region, where $\theta_{0–10}$ layer declined by 0.05 m^3 m^{-3} (-24%). Although $\theta_{10–20}$ declined in both scenarios during this period, $\theta_{10–20}$ in the winter wheat region increased by 0.02 m^3 m^{-3} (11%) in the Early Harvest scenario relative to the Late Harvest scenario. There was no significant difference between scenarios in the non-winter wheat region.

The Early Harvest scenario 2 m air and soil temperatures continued to warm

throughout Phase 2 relative to the Late Harvest scenario. Diurnal temperature range increased, as the increase in midday temperature was greater than the increase in nighttime temperature. In the winter wheat region, midday soil and 2 m air temperatures increased by 2.5°C and 1.3°C, respectively. The decline in latent heat flux during this phase resulted in warmer soil and a subsequent increase in sensible heat flux and air temperature. Warmer soil temperatures during the day resulted in warmer air temperatures at night. Midday soils warmed slightly (0.2°C) in the non-winter wheat region, but there was no significant difference in air temperature between scenarios.

Phase 3 was characterized by moderate differences between scenarios in ecosystem stocks and fluxes, but of the opposite sign of those in Phase 2. The latent heat flux increased in both scenarios throughout Phase 3. In the winter wheat region, midday latent heat flux increased by 74 W m^{-2} (20%), and sensible heat flux decreased by 17 W m^{-2} (-17%) in the Early Harvest relative to the Late Harvest scenario. At midday in the non-winter wheat region, both latent and sensible heat fluxes increased by 4 W m^{-2}. The increase in latent heat flux was due to enhanced precipitation in both scenarios during Phase 3. Precipitation increased soil moisture such that more water was available for evaporation. Slightly more precipitation occurred in the Early Harvest scenario (0.3 cm), resulting in greater latent heat flux. The additional precipitation in both scenarios reduced differences in $\theta_{0–10}$ and $\theta_{10–20}$.

In Phase 3, there was a slight cooling (0.2°C) in 2 m air temperature in the winter wheat region due to increased latent heat flux. Midday soil temperature was slightly warmer (0.8°C) in the winter wheat region. The reduction in the difference between scenarios in soil and air temperature was associated with an increase in precipitation

(Figure 9). Although latent heat flux increased as a result of precipitation, soil temperature remained warmer in the Early Harvest scenario. Because soil moisture in the Early Harvest scenario was low and drier soils warm easily, increases in latent heat flux in the Early Harvest scenario were not sufficient to cool the soil. The difference in soil temperature between scenarios, however, declined.

Differences between the two scenarios in Phase 4 were small. Precipitation during Phase 3 reduced soil moisture differences between scenarios such that when winter wheat was harvested in the Late Harvest scenario, the land surface in both scenarios was nearly identical. Thus, there was no significant difference in midday latent and sensible heat fluxes between the harvest scenarios. Differences in soil and 2 m air temperatures approached zero. There was no additional difference in precipitation between the two scenarios after Julian Day 200 (Figure 6). Although the regional average increase in precipitation was small (0.3 cm) over the two-month simulation, some areas received up to 13 cm more precipitation and others 15 cm less in the Early Harvest scenario relative to the Late Harvest scenario (Figure 10). This amounts to a significant redistribution of precipitation. Because we forced the domain boundaries with atmospheric liquid and vapor contents, we may have minimized differences in precipitation between scenarios. Enhanced exchange of soil moisture to the atmosphere resulted in all of the difference in cumulative precipitation. The rapid convergence for all ecosystem water pools and fluxes in the Early and Late Harvest scenarios indicates that the system had little or no memory of the previous month's harvest.

4.3. *Edge Effect and Spatial Variation*

There was considerable spatial heterogeneity in net ecosystem latent and sensible

heat fluxes, soil moisture and temperature, and 2 m air temperature in the response to harvest. As an example, consider differences in midday sensible heat flux on Julian Day 163, eight days after the June harvest. As shown in Figure 11, little or no change occurred in half of the domain, but the winter wheat region experienced a very large average increase of 250 W m^{-2} in midday sensible heat flux. Changes in the center of the winter wheat region, with sensible heat flux reaching a peak difference of 475 W m^{-2}, were greater than on the edges.

Although changes were largest within the winter wheat region, there was an edge effect, in which the impact of the harvest was felt in areas adjacent to the harvested, winter wheat region. In the example shown in Figure 11, increases in sensible heat flux in the winter wheat area resulted in the advection of warmer, drier air to the surrounding non-winter wheat area. The warm, dry air resulted in increases in latent heat fluxes in the surrounding non-winter wheat area. In the adjacent area, midday sensible heat flux declined by up to 50 W m^{-2} and latent heat flux increased. This effect was more pronounced to the East of the harvested region, which was downwind on this particular day. The surrounding non-harvested region, extending up to 60 km from the harvested region, absorbed the majority of the changes resulting from harvest that were communicated to the atmosphere. Within the harvested area itself, there was also a gradient in impacts, between the center and edge of the harvested region, such that the largest differences are found in the center of the harvested area. This gradient is established because of the ameliorating impacts of the surrounding non-harvest area on the edges inside the harvested area.

5. Discussion

Harvest dramatically alters energy, momentum, and water fluxes between the surface and atmosphere. These effects are comparable in magnitude to those predicted for land cover conversion by previous studies. We found a 1.3°C warming in midday air temperature during the first two weeks following harvest. In a ten-year climate simulation, Bonan [1999] found that conversion from forest to crop resulted in a decline in midday temperature of 0.6–1°C and 1–3°C in the East and Midwest, respectively. In a similar study, Bounoua et al. [2002] reported a 0.7–1.1°C decline in temperate regions due to land cover conversion. Our findings suggest that realistic harvest scenarios should be an integral part of climate model studies.

There were qualitative changes in the sign of the response to harvest over time. Transitions between the four temporal phases following harvest resulted from changes in water availability and subsequent effects on energy partitioning. Harvest initially caused an increase in latent heat flux and subsequent cooling of soil temperature. As soil temperature declined, sensible heat flux and air temperature also declined. These effects were reversed after three days, as soil moisture declined (Phase 2). Because the Early Harvest soil was drier during this period, latent heat flux was suppressed leading to warmer soil and a subsequent increase in sensible heat flux and air temperature. As precipitation increased, the difference in soil moisture declined (Phase 3). During Phase 3, sufficient soil moisture was available to drive increases in latent heat flux and reduce the difference in soil temperature between scenarios. Harvest thus caused large shifts in energy partitioning, which led to changes in soil moisture and air and soil temperatures. Changes in soil moisture in turn caused further changes in energy partitioning. After

precipitation occurred in both scenarios, albeit in different amounts, the differences between scenarios declined.

If the early harvest had occurred during a wet period, a much simpler response pattern would have emerged. Phase 2 was a result of a lack of soil moisture and subsequent suppression of latent heat flux. If water was available in abundance, we would likely have seen elevated latent heat fluxes in the Early Harvest scenario throughout the simulation, as seen in Phases 1 and 3 but not Phase 2.

These results suggest that harvest should be examined under different climatic regimes, particularly during prolonged dry periods. The variability in system response through time also highlights the importance of running longer simulations. If we had only examined a two-week simulation, we would not have observed the qualitative shifts in energy partitioning or the re-equilibration of the system after the second harvest.

Although the model predicted that harvest has little long-term impact on the system, harvest likely causes secondary effects not explored here. The substantial drying of the 0–10 cm soil layer during Phase 1 and changes in soil moisture and air and soil temperatures throughout the simulations influence microbial processes, decomposition, and trace-gas fluxes. These processes also influence the isotopic composition of evaporated water and CO_2 [*Riley et al.*, 2002]. In addition, a dry soil surface may promote aeolian erosion and thereby impact air quality.

6. Conclusions

Our findings improve the understanding of the impacts of temporally coherent harvesting and subsequent soil and atmospheric conditions within and outside of the

harvested area. We note that changes identified in this study are analogous to changes that may occur as crops shift to an earlier growing season in response to global warming.

We observed that an early harvest, which is prompted by hot, dry conditions, could substantially exacerbate these conditions within the harvested area. Farmers adjacent to the harvested area can also be adversely impacted. Collective decision-making and land management techniques, such as mulching or leaving stubble on the soil, may mitigate the adverse impacts observed here. Agricultural decision-making is dependent upon a number of factors, including expected returns on investments, labor and machinery availability, current market conditions, and uncertainty estimates. Thus, while we have shown that an early harvest exacerbates hot, dry conditions, it is important to realize that the decision of harvest timing is constrained.

We have shown that land management has an impact on climate comparable to that reported for land use and land cover change. To the extent that management is influenced by short-term climatic or weather conditions, these practices form important feedbacks with regional climate.

7. Acknowledgments

This work was supported by the Laboratory Directed Research and Development Program at Lawrence Berkeley National Laboratory and the Atmospheric Radiation Measurement Program, Office of Science, U.S. Department of Energy under Contract No. DE-AC03-76SF00098. The leaf area index (LAI) data used here were obtained in a field study supported by the Office of Biological and Environmental Research (BER), U.S. Department of Energy, through the Great Plains Regional Center of the National

Institute for Global Environmental Change (NIGEC) under Cooperative Agreement No. DE-FC03-90ER61010.

8. References

Betts, A.K., and J.H. Ball, Fife Surface Climate and Site-Average Dataset 1987–89, *Journal of the Atmospheric Sciences*, *55* (7), 1091–1108, 1998.

Bonan, G.B., A land surface model (LSM version 1.0) for ecological, hydrological, and atmospheric studies: Technical description and user's guide, pp. 150, NCAR, Boulder, CO, 1996.

Bonan, G.B., Effects of land use on the climate of the United States, *Climatic Change*, *37*, 449–486, 1997.

Bonan, G.B., Frost followed the plow: impacts of deforestation on the climate of the United States, *Ecological Applications*, *9* (4), 1305–1315, 1999.

Bonan, G.B., F.S. Chapin, III, and S.L. Thompson, Boreal forest and tundra ecosystems as components of the climate system, *Climatic Change*, *29*, 145–168, 1995.

Bonan, G.B., K.J. Davis, D. Baldocchi, D. Fitzgerald, and H. Neumann, Comparison of the NCAR LSM I land surface model with BOREAS aspen and jack pine tower fluxes, *Journal of Geophysical Research*, *102* (C12), 29,065–29,076, 1997.

Bounoua, L., R. DeFries, G.J. Collatz, P. Sellers, and H. Khan, Effects of land cover conversion on surface climate, *Climatic Change*, *52*, 29–64, 2002.

Chase, T.N., R.A.P. Sr., T.G.F. Kittel, J.S. Baron, and T.J. Stohlgren, Potential impacts on Colorado Rocky Mountain weather due to land use changes on the

adjacent Great Plains, *Journal of Geophysical Research*, *104* (D4), 16,673–16,690, 1999.

Chen, F., and J. Dudhia, Coupling an advanced land surface-hydrology model with the Penn State-NCAR MM5 modeling system. Part I: Model implementation and sensitivity, *Monthly Weather Review*, *129* (4), 569–585, 2001a.

Chen, F., and J. Dudhia, Coupling an advanced land surface-hydrology model with the Penn State-NCAR MM5 modeling system. Part II: Preliminary model validation, *Monthly Weather Review*, *129* (4), 587–604, 2001b.

Copeland, J.H., R.A. Pielke, and T. Kittel, Potential climatic impacts of vegetation change: a regional modeling study, *Journal of Geophysical Research*, *101* (D3), 7409–7418, 1996.

DeFries, R.S., L. Bounoua, and J. Collatz, Human modification of the landscape and surface climate in the next fifty years, *Global Change Biology*, *8*, 438–458, 2002.

Dickinson, R.E., A. Henderson-Sellers, P.J. Kennedy, and M.F. Wilson, *Biosphere/atmosphere transfer scheme (BATS) for the NCAR community climate model. NCAR Technical Note TN275*, National Center For Atmospheric Research, Boulder, Colorado, 1986.

Garratt, J.R., Sensitivity of climate simulations to land-surface and atmospheric boundary-layer treatments-a review, *Journal of Climate*, *6*, 419–449, 1993.

Grell, G., J. Dudhia, and D. Stauffer, A description of the fifth-generation Penn State/NCAR mesoscale model (MM5), NCAR, Boulder, CO, 1995.

Loveland, T.R.a.H.L.H., Monitoring Changes in Landscapes from Satellite Imagery, in *Our Living Resources: A Report to the Nation on the Distribution, Abundance, and*

Health of U.S. Plans, Animals, and Ecosystems, edited by E.T. Laroe, G.S. Farris, C.E. Puckett, P.D. Doran, and M.J. Mac, U.S. Department of the Interior-National Biological Service, Washington D.C., 1995.

Lu, L., R.A.P. Sr., G.E. Liston, W.J. Parton, D. Ojima, and M. Hartman, Implementation of a two-way interactive atmospheric and ecological model and its application to the central United States, *Journal of Climate*, *14*, 900–919, 2001.

McPherson, R., David J. Stensrud, and Kenneth C. Crawford, The impact of Oklahoma's winter wheat belt on the mesoscale environment, *Monthly Weather Review*, *132* (2), 405–421, 2004.

Ostlie, W.R., Rick E. Schneider, Janette Marie Aldrich, Thomas M. Faust, Robert L.B. McKim, and Stephen J. Chaplin, The Status of Biodiversity in The Great Plains, pp. 325, The Nature Conservancy, Minneapolis, 1997.

Pan, Z., E. Takle, M. Segal, and R. Arritt, Simulation of potential impacts of man-made land use changes on U.S. summer climate under various synoptic regimes, *Journal of Geophysical Research*, *104* (D6), 6515–6528, 1999.

Pielke, R.A., and R. Avissar, Influence of landscape structure on local and regional climate, *Landscape Ecology*, *4* (2/3), 133–155, 1990.

Pielke, R.A., D.S. Schimel, T.J. Lee, T.G.F. Kittel, and X. Zeng, Atmosphere-terrestrial ecosystem interactions: implications for coupled modeling, *Ecological Modeling*, *67*, 5–18, 1993.

Pielke, R.A.S., R. Avissar, M. Raupack, A.J. Dolman, X. Zeng, and A.S. Denning, Interactions between the atmosphere and terrestrial ecosystems: influence on weather and climate, *Global Change Biology*, *4*, 461–475, 1998.

Riley, W.J., C.J. Still, M.S. Torn, and J.A. Berry, A mechanistic model of $H_2{}^{18}O$ and $C^{18}OO$ fluxes between ecosystems and the atmosphere: Model description and sensitivity analyses, *Global Biogeochemical Cycles*, *16*, 1095–1109, 2002.

Riley, W.J., C.S. Still, B.R. Helliker, M. Ribas-Carbo, S. Verma, and J.A. Berry, Measured and modeled $\delta^{18}O$ in CO_2 and H_2O above a tallgrass prairie, *Global Change Biology*, *in press*, 2003.

Samson, F., and F. Knopf, Prairie conservation in North America, *Bioscience*, *44* (6), 418–421, 1994.

Segal, M., Z. Pan, R.W. Turner, and E.S. Takle, On the potential impact of irrigated areas in North America on summer rainfall caused by large-scale systems, *Journal of Applied Meteorology*, *37*, 325–331, 1998.

Sellers, P.J., D.A. Randall, C.J. Collatz, J.A. Berry, C.B. Field, D.A. Dazlich, C. Zhang, and G.D. Colello, A revised land surface parameterization (SiB2) for atmospheric GCMs. Part 1: Model formulation, *Journal of Climate*, *9*, 676–705, 1996.

USDA, 1997 Census of Agriculture, U.S. Department of Agriculture National Agricultural Statistics Service, 1997a.

USDA, Usual Planting and Harvesting Dates for U.S. Field Crops, US Department of Agriculture National Agricultural Statistics Service, 1997b.

Vitousek, P.M., Beyond global warming: ecology and global change, *Ecology*, *75* (7), 1861–1876, 1994.

Weaver, C.P., and R. Avissar, Atmospheric disturbances caused by human modification of the landscape, *Bulletin of the American Meteorological Society*, *82* (2), 269–281, 2001.

9. Figure Captions

Figure 1. Dominant land cover types across the ARM-CART determined from 1992 USGS 1-km AVHRR and 1997 USDA agricultural census data. The dominant land cover types are represented as the following: orange = winter wheat, purple = other crops, yellow = pasture/grassland, blue = savannah. A black line at 37° separates Oklahoma and Kansas. Note that winter wheat occurs in a nearly contiguous belt in the center of the region.

Figure 2. Green and total leaf area index for (a) winter wheat and (b) other crops. The values for winter wheat are from the Ameriflux site in Ponca City, OK and those for the other crops are prescribed by LSM1.

Figure 3. Comparison between FIFE measurements and the MM5/LSM and MM5/OSULSM predictions for June 1987. Shown are the (a) latent, (b) sensible, and (c) ground heat fluxes.

Figure 4. Comparison between FIFE measurements and the MM5/LSM and MM5/OSULSM predictions for June 1987. Shown are the surface skin and 2 m air temperatures.

Figure 5. Predicted latent and sensible heat fluxes over the simulation period. Panels show the (a) latent and (c) sensible heat fluxes for the Late Harvest scenario and the average difference (Early - Late Harvest scenario) in (b) latent and (d) sensible heat fluxes for the winter wheat and non-winter wheat land cover types. Patterns in sensible heat flux mirror those in latent heat flux.

Figure 6. Cumulative precipitation over the simulation period. Panels show the (a) cumulative precipitation for the Late Harvest scenario and (b) the regional average of the difference (Early-Late Harvest scenario) in cumulative precipitation. Each vertical jump in cumulative precipitation represents a rain event. Note that there was an initial dry period, followed by a wet period.

Figure 7. Soil moisture in the 0-10 and 10-20 cm layer over the simulation period. Panels show the (a and c) soil moisture in the Late Harvest scenario and the (b and d) average difference (Early - Late Harvest scenario) in soil moisture for the winter wheat and non-winter wheat land cover types. Initial changes in the 0-10 cm layer are opposite those in the 10-20 cm layer.

Figure 8. 2 m air temperature and soil temperature in the 0-10 cm layer over the simulation period. Panels show the (a) air and (c) soil temperature for the Late Harvest

scenario and the average difference (Early - Late Harvest scenario) in (b) air and (d) soil temperature for the winter wheat and non-winter wheat land cover types. For both variables, there was an initial cooling, followed by a prolonged warm period. This warming is interrupted on Julian Day 170, corresponding to an increase in precipitation.

Figure 9. Average cumulative precipitation across the region and the difference in soil and air temperatures over the simulation period. Differences in soil and air temperature are averaged for the winter wheat land cover type. System response was closely tied to precipitation patterns. System response was greatest during the two-week dry period following harvest. After the onset of rainfall, differences between scenarios approached zero.

Figure 10. Changes in cumulative precipitation (cm) across the ARM-CART. Although the average difference between scenarios was small (0.3 cm), some areas experienced large changes in cumulative precipitation.

Figure 11. Changes in sensible heat flux (W m^{-2}) across the region on Julian Day 163. Little or no change occurred in half of the domain, but the winter wheat region experienced very large average increases of 250 W m^{-2} in midday sensible heat fluxes. Changes were largest in the center of the winter wheat region, with sensible heat flux reaching a peak difference of 475 W m^{-2}. Changes were also evident along the edges of the harvested area, indicating an edge effect. This effect was more pronounced to the East in accordance with the prevailing winds during this period.

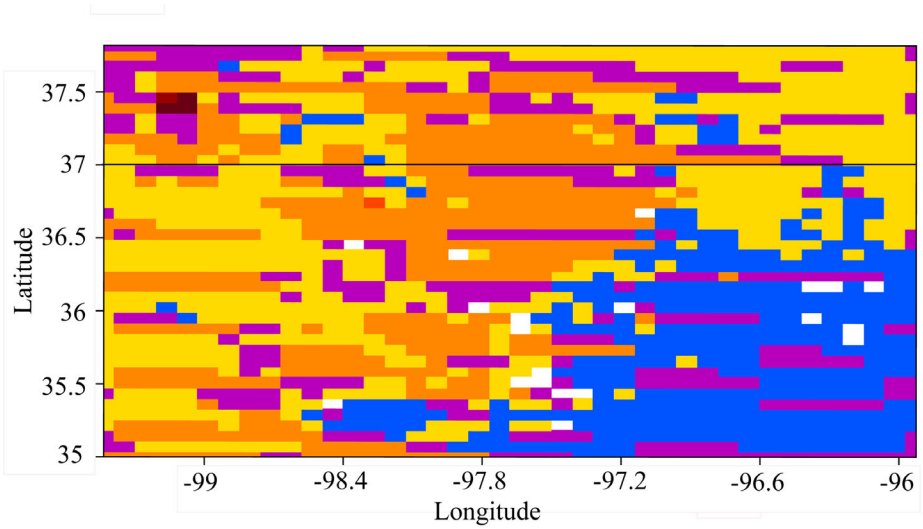

Figure 1. Dominant land cover types across the ARM-CART determined from 1992 USGS 1-km AVHRR and 1997 USDA agricultural census data. The dominant land cover types are represented as the following: orange = winter wheat, purple = other crops, yellow = pasture/grassland, blue = savannah. A black line at 37° separates Oklahoma and Kansas. Note that winter wheat occurs in a nearly contiguous belt in the center of the region.

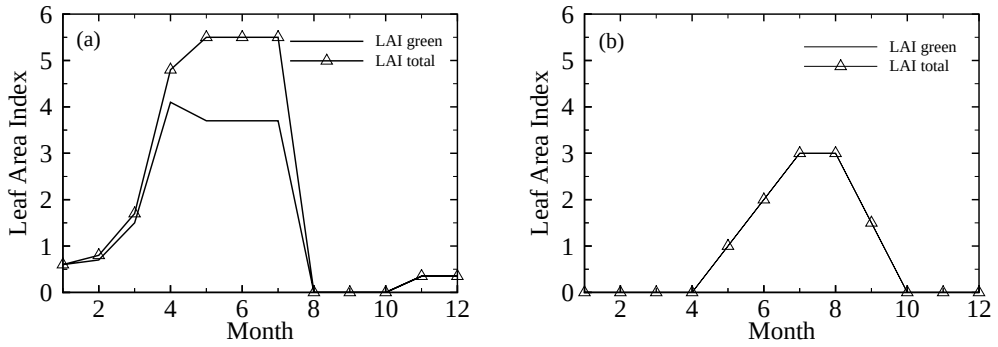

Figure 2. Green and total leaf area index for (a) winter wheat and (b) other crops. The values for winter wheat are from the Ameriflux site in Ponca City, OK and those for the other crops are prescribed by LSM1.

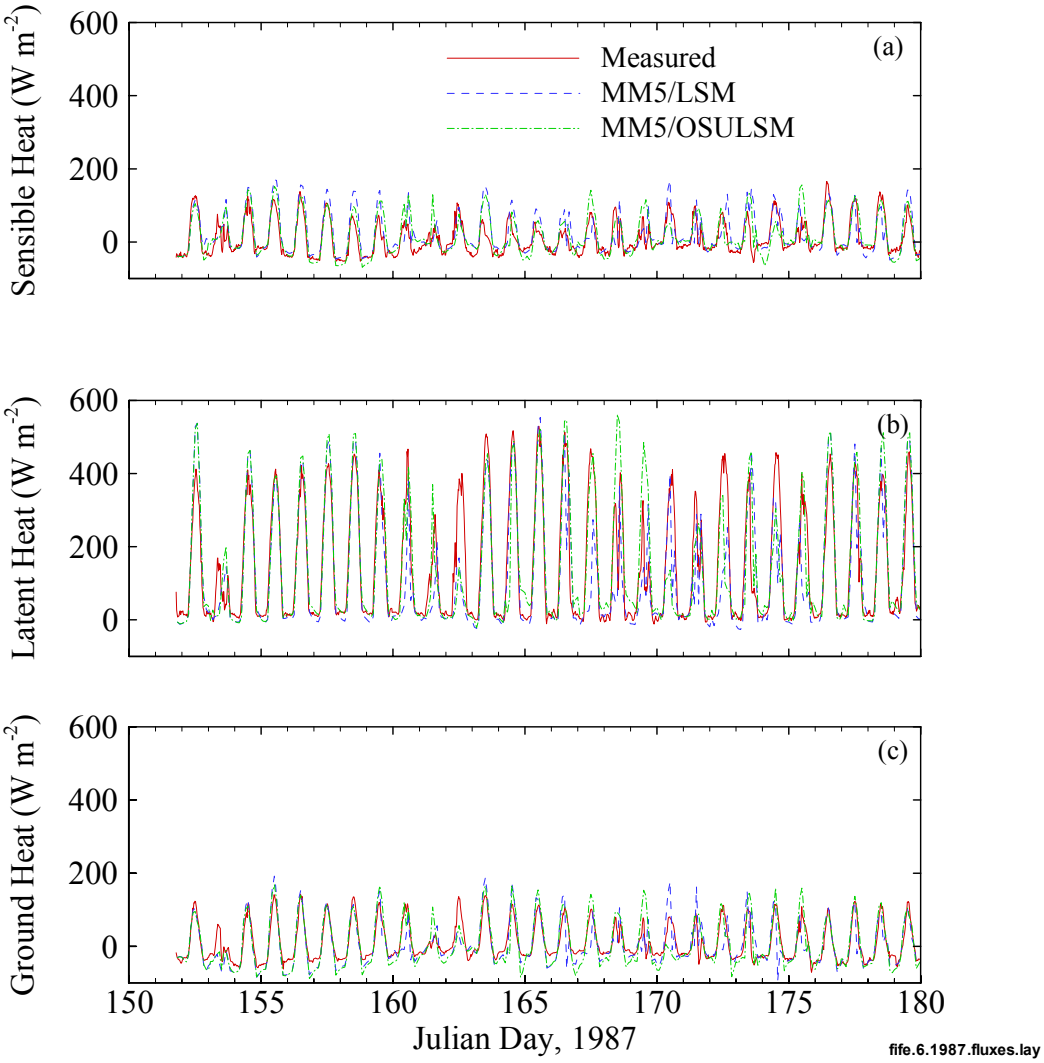

Figure 3. Comparison between FIFE measurements and the MM5/LSM and MM5/OSULSM predictions for June 1987. Shown are the (a) latent, (b) sensible, and (c) ground heat fluxes.

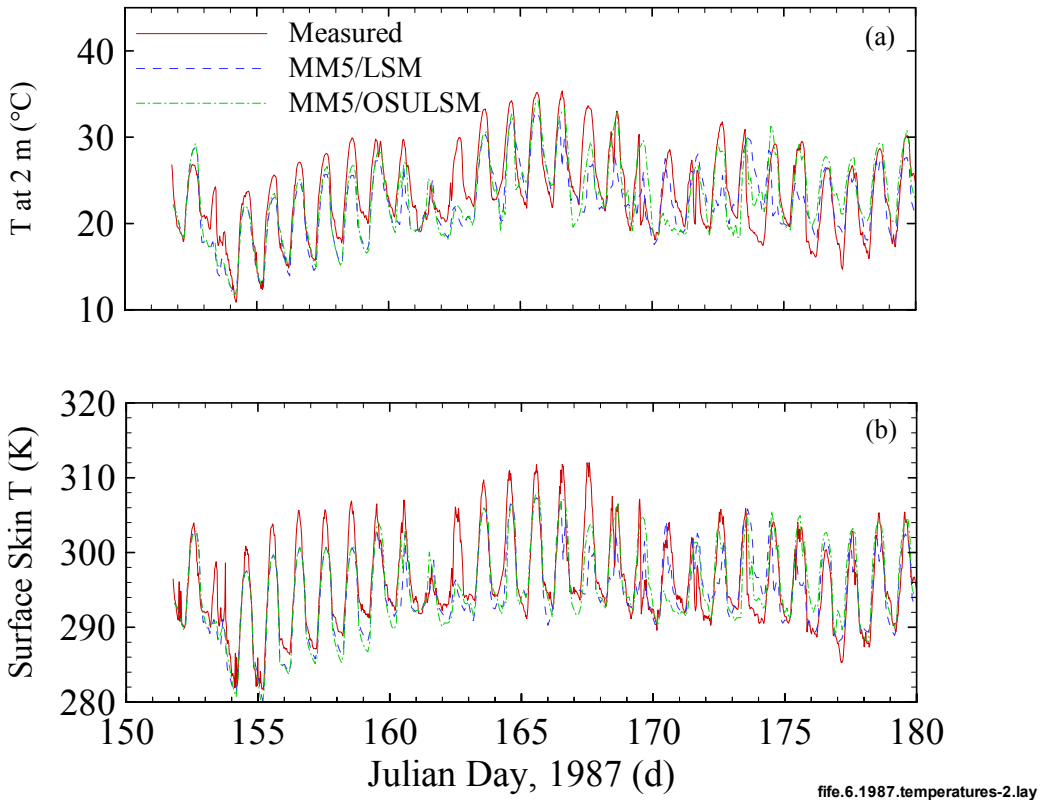

Figure 4. Comparison between FIFE measurements and the MM5/LSM and MM5/OSULSM predictions for June 1987. Shown are the surface skin and 2 m air temperatures.

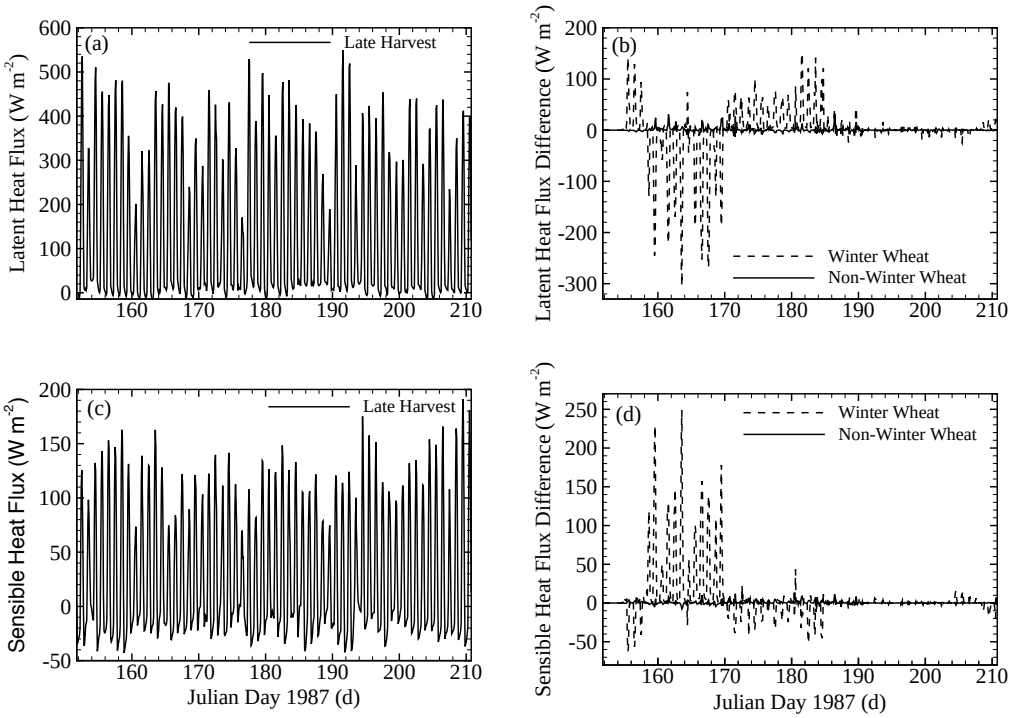

Figure 5. Predicted latent and sensible heat fluxes over the simulation period. Panels show the (a) latent and (c) sensible heat fluxes for the late harvest scenario and the average difference (early - late harvest scenario) in (b) latent and (d) sensible heat fluxes for the winter wheat and non-winter wheat land cover types. Patterns in sensible heat flux mirror those in latent heat flux.

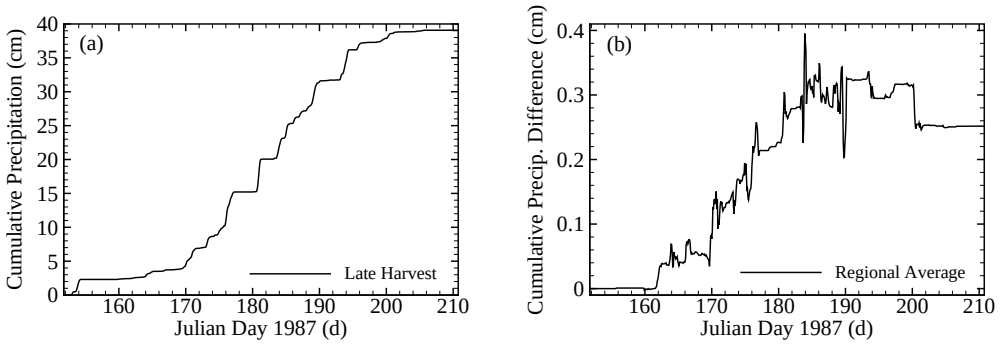

Figure 6. Cumulative precipitation over the simulation period. Panels show the (a) cumulative precipitation for the late harvest scenario and (b) the regional average of the difference (early-late harvest scenario) in cumulative precipitation. Each vertical jump in cumulative precipitation represents a rain event. Note that there was an initial dry period, followed by a wet period.

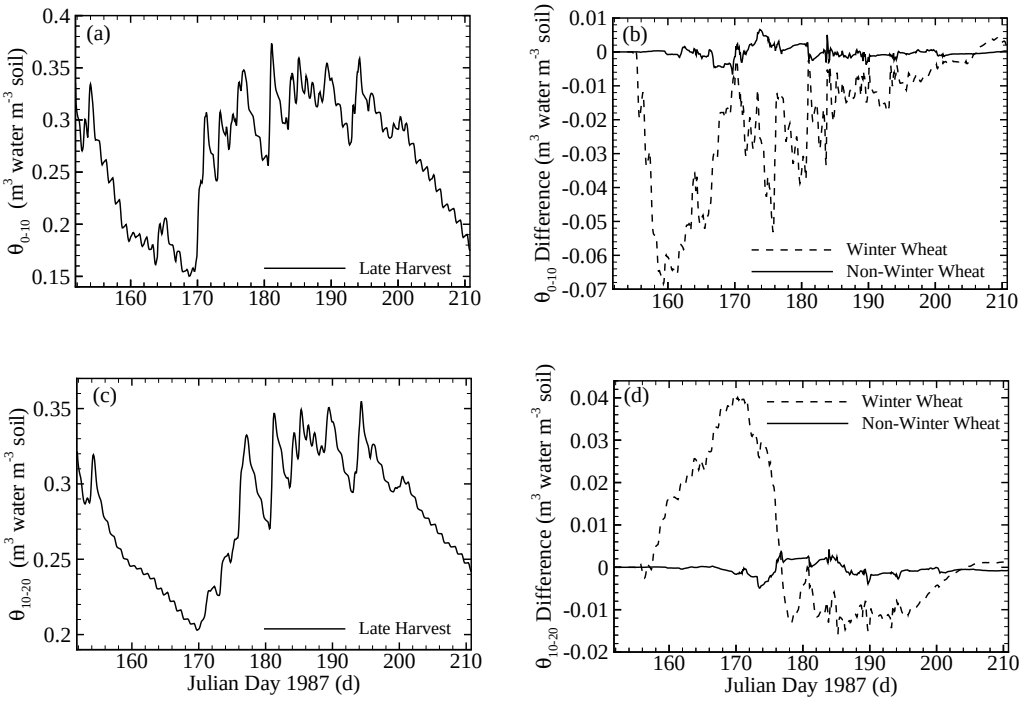

Figure 7. Soil moisture in the 0-10 and 10-20 cm layer over the simulation period. Panels show the (a and c) soil moisture in the late harvest scenario and the (b and d) average difference (early - late harvest scenario) in soil moisture for the winter wheat and non-winter wheat land cover types. Initial changes in the 0-10 cm layer are opposite those in the 10-20 cm layer.

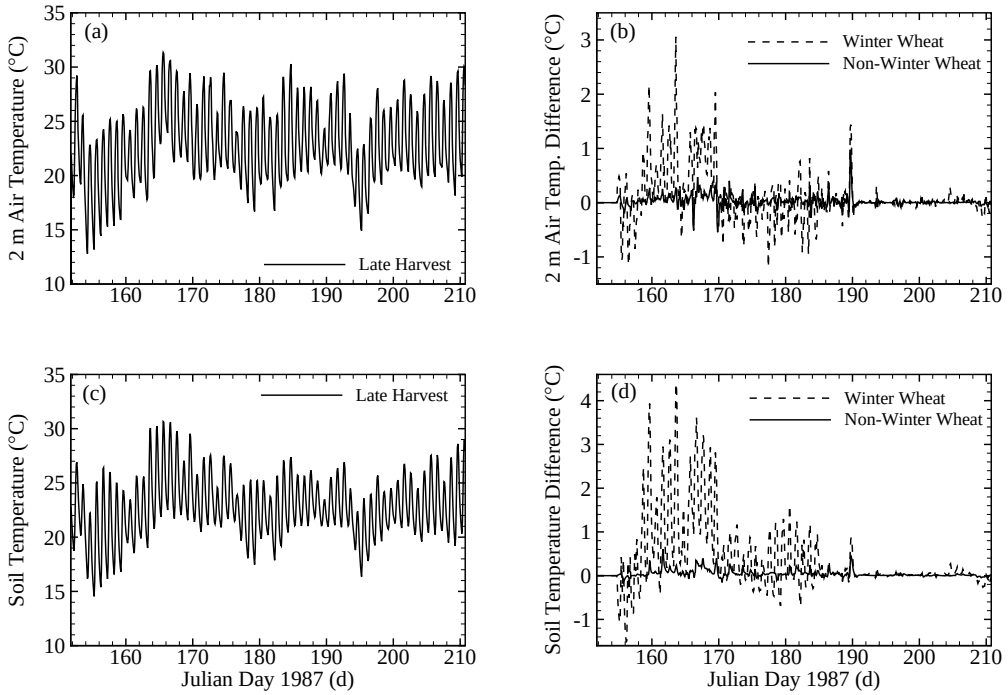

Figure 8. 2 m air temperature and soil temperature in the 0-10 cm layer over the simulation period. Panels show the (a) air and (c) soil temperature for the late harvest scenario and the average difference (early - late harvest scenario) in (b) air and (d) soil temperature for the winter wheat and non-winter wheat land cover types. For both variables, there was an initial cooling, followed by a prolonged warm period. This warming is interrupted on Julian Day 170, corresponding to an increase in precipitation.

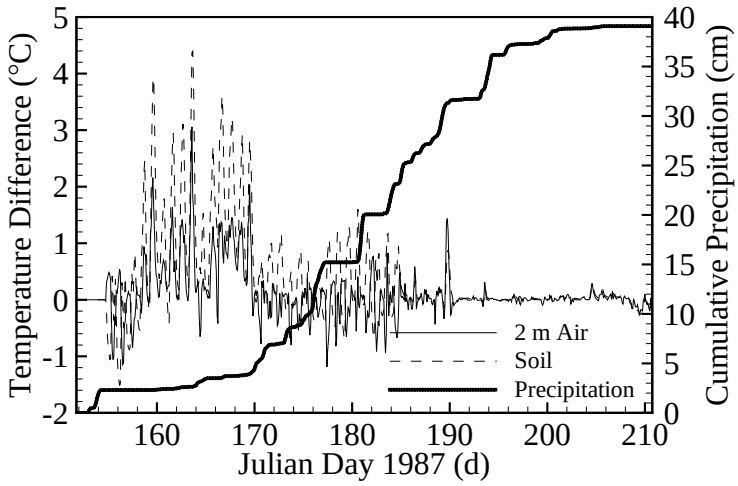

Figure 9. Average cumulative precipitation across the region and the difference in soil and air temperatures over the simulation period. Differences in soil and air temperature are averaged for the winter wheat land cover type. System response was closely tied to precipitation patterns. System response was greatest during the two-week dry period following harvest. After the onset of rainfall, differences between scenarios approached zero.

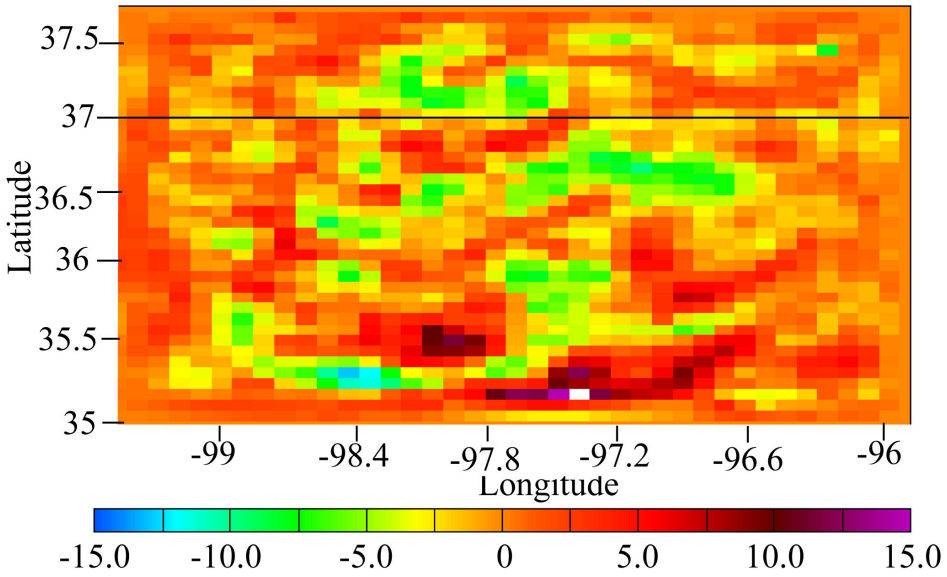

Figure 10. Changes in cumulative precipitation (cm) across the ARM-CART. Although the average difference between scenarios was small (0.3 cm), some areas experienced large changes in cumulative precipitation.

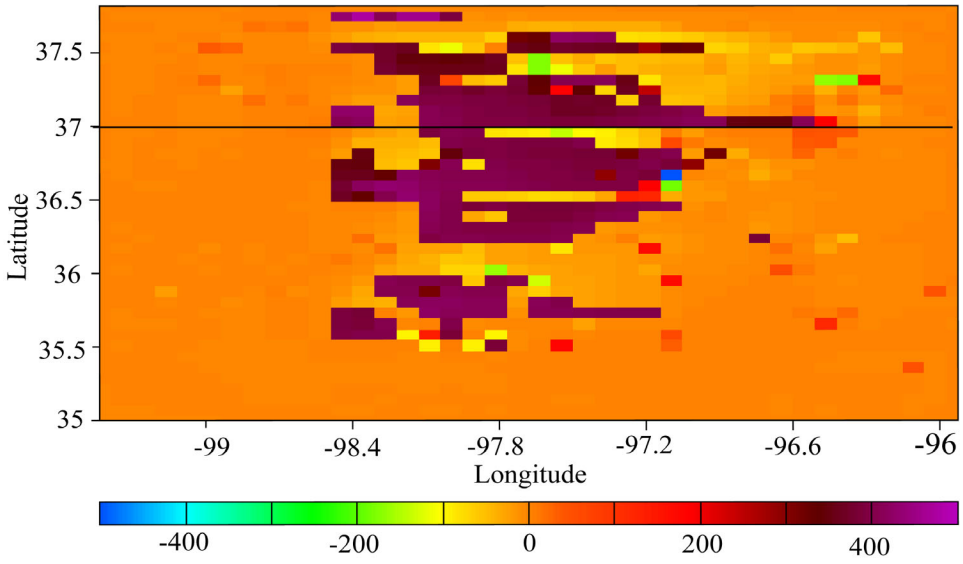

Figure 11. Changes in sensible heat flux (W m^{-2}) across the region on Julian Day 163. Little or no change occurred in half of the domain, but the winter wheat region experienced very large average increases of 250 W m^{-2} in midday sensible heat fluxes. Changes were largest in the center of the winter wheat region, with sensible heat flux reaching a peak difference of 475 W m^{-2}. Changes were also evident along the edges of the harvested area, indicating an edge effect. This effect was more pronounced to the East in accordance with the prevailing winds during this period.